Proton formation dynamics in the REMPI[2+n] process via the F $^1\Delta_2$ and f $^3\Delta_2$ Rydberg states of HCl investigated by three-dimensional velocity mapping

S. Kauczok,[1,a)] C. Maul,[1] A. I. Chichinin,[2] and K.-H. Gericke[1]
[1]*Institut für Physikalische und Theoretische Chemie, TU Braunschweig, 38106 Braunschweig, Germany*
[2]*Institute of Chemical Kinetics and Combustion, 630090 Novosibirsk, Russia*

(Received 29 January 2010; accepted 15 April 2010; published online 9 July 2010)

HCl in the bulk gas phase at a pressure of 10^{-5} mbar has been excited via selected Q-lines of the two-photon transition band systems F $^1\Delta_2 \leftarrow$ X $^1\Sigma^+(1,0)$ [Q(8)], V $^1\Sigma^+ \leftarrow$ X $^1\Sigma^+(14,0)$ [Q(8), Q(7)] and f $^3\Delta_2 \leftarrow$ X $^1\Sigma^+(0,0)$ [Q(2–6)]. Concerning the V $\leftarrow$ X excitation, subsequent photon absorption is known to yield HCl^+, H(n=2)+Cl, $H^+ + Cl^-$ and H+Cl(4s,4p,3d). Vibrationally excited HCl^+ ($v^+ \geq 5$) can be photodissociated to H^++Cl, and excited atoms can be easily photoionized by absorption of a fourth photon, respectively. Using three-dimensional velocity map imaging, the spatial proton velocity distributions resulting from these processes for these particular transitions were studied for the first time. Kvaran *et al.* [J. Chem. Phys. **131**, 044324 (2009); J. Chem. Phys. **129**, 164313 (2008)] recently reported a substantial increase in the formation of chlorine and hydrogen ions in single rovibrational transitions of the F $^1\Delta_2$ and f $^3\Delta_2$ band systems using mass resolved resonance enhanced multiphoton ionization spectroscopy and explained this by the vicinity of single rovibrational levels of the V $^1\Sigma^+$ state for which photorupture is the main feature. Thus, the known dissociation dynamics of the V $^1\Sigma^+$ state should also leave their fingerprint in the spatial proton velocity distribution emerging from the photodissociation of those states. Accordingly, we found a strong increase in the H^+ ion signal for the Q(5) line of the f $^3\Delta_2 \leftarrow$ X $^1\Sigma^+(0,0)$ transition, the extra signal resulting from dissociation into H(n=2)+Cl($^2P_{1/2}$) and the ion pair. No increase for the $HCl^+(v^+ \geq 5)$ photodissociation channel or dissociation into H(n=2)+Cl($^2P_{3/2}$) has been observed. Furthermore, H^+ distributions from the Q transitions of the f $^3\Delta_2 \leftarrow$ X $^1\Sigma^+(0,0)$ band system were found to show the two features previously ascribed to the "gateway" state $[^4\Pi \cdots 4s]^3\Pi(0)$, i.e., autoionization into $HCl^+(5 \leq v^+ \leq 8)$ and nonadiabatic dissociation into H(n=2)+Cl($^2P_{3/2}$). The F $^1\Delta_2 \leftarrow$ X $^1\Sigma^+(1,0)$ band system only showed significant proton formation for the Q(8) line. The speed distribution is the same as for the Q(8,7) lines of the V $^1\Sigma^+ \leftarrow$ X $^1\Sigma^+(14,0)$ transition while the excitation history is conserved in the angular distribution confirming the resonance interpretation. © *2010 American Institute of Physics*.
[doi:10.1063/1.3427541]

I. INTRODUCTION

The excited states and the dynamics involved in the photodissociation and photoionization of the HCl molecule and the corresponding ion HCl^+ have been the subject of a large number of spectroscopic and theoretical investigations.[1–20] Studies investigating the resonance enhanced multiphoton ionization (REMPI)[10–20] have revealed fascinating dynamics involving highly excited Rydberg states above the ionization limit. Particularly, the photodissociation and autoionization as well as the subsequent photodissociation of the highly vibrationally excited molecular ion HCl^+ following the two-photon excitation to the B $^1\Sigma^+$ state have been of special interest. Usually, 2+n REMPI (n=1,2) of the HCl molecule via pure low lying Rydberg states is known to lead to direct ionization only, leaving the HCl^+ ion in the lowest vibrational states. This cannot be photodissociated in a one-photon step at the wavelengths involved. In contrast, the B $^1\Sigma^+$ double minimum state resulting from an avoided crossing of the E $^1\Sigma^+$ Rydberg and the V $^1\Sigma^+$ state is known to undergo photodissociation in competition to the direct ionization. The V $^1\Sigma^+$ state is itself the result of an avoided crossing of a valence state and the ion-pair state asymptotically correlated with H^+ and Cl^- (Fig. 1).[8,21,22] A number of channels for the photodissociation has recently been identified by photoion and photoelectron imaging methods, both for the Cl^+ and the H^+ products [Eq. (1)].[13,14,19,20]

$$\mathrm{HCl} \xrightarrow{2h\nu} \mathrm{HCl(B\ ^1\Sigma^+)} \xrightarrow{h\nu} \begin{cases} \mathrm{HCl^+(v^+ \leq 12) + e^-} \\ \mathrm{HCl^{**}} \\ \mathrm{H^+ + Cl^-} \end{cases} \xrightarrow{h\nu} \begin{cases} \mathrm{H^+ + Cl + e^-} \\ \mathrm{H + Cl^+ + e^-} \end{cases} . \quad (1)$$

It has been shown that the speed distribution of the H^+ ions always shows three global features only shifting in energy and changing in their relative intensities when the wave-

[a)]Electronic mail: s.kauczok@tu-bs.de.

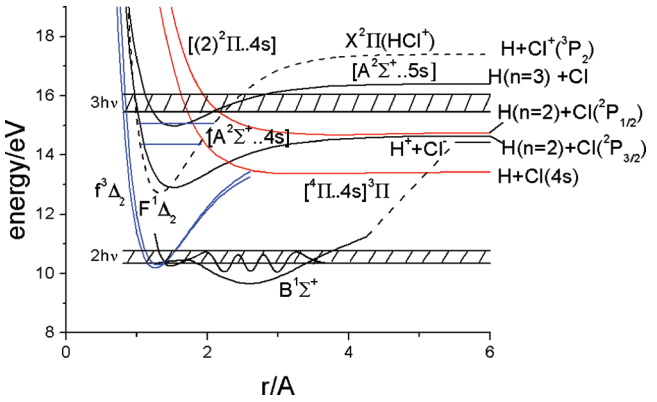

FIG. 1. Relevant potential energy curves. The B $^1\Sigma^+$ state has been reproduced from Ref. 30; the f $^3\Delta_2$ and F $^1\Delta_2$ states (blue) are represented by Morse potentials constructed from spectroscopic data in Refs. 10–12. The ground state of the ion (dashed) is the *ab initio* curve from Ref. 5 and is shown with the vibrational levels $v^+=5,8$. The hatched areas show the two- and three-photon energies for the two bands investigated (lower bound: f $^3\Delta_2$, upper bound: F $^1\Delta_2$). The dissociative Rydberg states (red) have been obtained by shifting the *ab initio* curves from Pradhan *et al.* to their respective asymptotes. The Rydberg states with A $^2\Sigma^+$ core have been constructed from the ionic *ab initio* curve in Ref. 5 and the quantum defects reported in Ref. 7. The wave function has been obtained by the Numerov method for the potential of Bruna *et al.* (Ref. 30) for the eigenvalue closest to the two-photon energy. Note that this is only a sketch of the reality as it has only six nodes. However, it illustrates the principal circumstances very well (see text).

length is changed.[13,14,19,20] These three features are all attributed to the accessibility of the outer well of the V $^1\Sigma^+$ state and they constitute the formation of (1) excited H atoms (n=2) with the partner fragment mostly in the spin orbit excited state $^2P_{1/2}$, (2) dissociation into the ion-pair, and (3) photodissociation of autoionized HCl^+ in the X $^2\Pi_\Omega$ state vibrationally excited to $v^+=5-8,12-14$. Eqs. (2)–(4) sum up the different channels that are thus far believed to play the key role in the production of the H^+ distribution showing these three features. The arguments that lead to this conclusion will be discussed in detail below (see Fig. 1 for the potential curves of the states involved).

$$\mathrm{HCl}(\mathrm{B}\ ^1\Sigma^+)\xrightarrow{h\nu}\mathrm{HCl}([^4\Pi\cdots 4s]^3\Pi_0)\rightarrow\begin{cases}\mathrm{HCl}^+(\mathrm{X}\ ^2\Pi, v^+\geq 5)+e^-\xrightarrow{h\nu}\mathrm{H}^+ + \mathrm{Cl}+e^-\\ \mathrm{H}(n=2)+\mathrm{Cl}(^2P_{3/2})\xrightarrow{h\nu}\mathrm{H}^+ + \mathrm{Cl}+e^-\\ \mathrm{H}+\mathrm{Cl}(4s)\xrightarrow{h\nu}\mathrm{Cl}^+ + \mathrm{H}+e^-\\ \mathrm{HCl}^+(\mathrm{X}\ ^2\Pi, v^+<5)+e^-,\end{cases}\tag{2}$$

$$\mathrm{HCl}(\mathrm{B}\ ^1\Sigma^+)\xrightarrow{h\nu}\mathrm{HCl}([(2)^2\Pi\cdots 4s]^1\Sigma_0,{}^3\Pi_0)\rightarrow \mathrm{H}(n=2)+\mathrm{Cl}(^2P_{1/2})\xrightarrow{h\nu}\mathrm{H}^+ + \mathrm{Cl}+e^-,\tag{3}$$

$$\mathrm{HCl}(\mathrm{B}\ ^1\Sigma^+)\xrightarrow{h\nu}\mathrm{HCl}[\mathrm{A}\ ^2\Sigma^+\cdots 5s\sigma 5p\sigma 4d\sigma]^1\Sigma(0)\rightarrow \mathrm{HCl}(\mathrm{V}\ ^1\Sigma^+)\rightarrow \mathrm{H}^+ + \mathrm{Cl}^-.\tag{4}$$

Photoelectron images measured by Romanescu *et al.* showed an oscillating behavior of the photoelectron intensities in the vibrational progression for $v^+>3$ in the autoionization process of HCl.[13] They concluded that the gateway state for the autoionization to HCl^+ (X $^2\Pi(v^+>3)$) is most likely the purely repulsive $^3\Pi(0)$ state having a $^4\Pi$ ion core and a 4sσ Rydberg electron (see Fig. 1 for the states involved in the following discussion). The lower vibrational states of $HCl^+(\mathrm{X}\ ^2\Pi, v^+<3)$ are likely to be populated by direct ionization. This gateway state converges to ground state H atoms and excited Chlorine Cl(4s) and crosses the $[\mathrm{A}\ ^2\Sigma^+\cdots 4s\sigma]^1\Sigma^+$ curve that converges to H(n=2) and $\mathrm{Cl}(^2P_{3/2})$. It has been estimated that ca. 5%–10% of the molecules excited to the gateway state proceed to form H(n=2)+$\mathrm{Cl}(^2P_{3/2})$.[14] Photoion images recorded by Romanescu *et al.* and in our group led to the conclusion that dissociation of HCl^+ upon absorption of a fourth photon can only occur in the vibrational states $v^+\geq 5$ through the repulsive state $(2)^2\Pi$ of HCl^+ (see Fig. 13 of Ref. 19 showing a plot of the dressed ionic ground state and its vibrational levels). The summary of this channel is given in Eq. (2).

The H(n=2) in coincidence with $\mathrm{Cl}(^2P_{1/2})$ atoms [see Eq. (3)] are formed primarily by excitation of an $\Omega=0$ Rydberg state belonging to the series with a repulsive $^2\Pi$ ion core ($^1\Sigma(0)$, $^3\Pi(0)$). $\Omega=0$ is indicated by the positive β-parameter. As usual, the β-parameter characterizes the angular distribution for a dipole transition by $P(\theta)=1/2(1+\beta\cdot P_2(\cos\theta))\cdot\sin\theta$, θ being the polar angle between the laser polarization and the recoil velocity vector.

The ion-pair channel [Eq. (4)] was first found by Yencha *et al.*[23] in one-photon processes using synchrotron radiation in the energy range 14.4–16.4 eV. Hepburn and co-workers[3,24] found similar results using threshold ion-pair production spectroscopy near 14.4 eV photon energy. The analysis of the results showed that the ion-pair is formed by the predissociation of Rydberg states with an A $^2\Sigma^+$ ion core and nlσ electrons (n=4–6) by the diabatic curve of the V $^1\Sigma^+$ ion-pair state. In the energy range of the REMPI process under scrutiny in this study, the formation of the ion-pair came unexpectedly when Romanescu *et al.* first observed it.[14] It is very intriguing that in this case the ion-pair yield is highest, when the intermediate state is the ion-pair state V($^1\Sigma^+$) itself. The previous results show unambiguously, and the present add strong evidence to it, that the ion-pair formation in this REMPI process is an exclusive feature of the outer well of the B $^1\Sigma^+$ state at the energies involved. As pointed out by Romanescu *et al.*, the Franck–Condon region for the excitation to the bound $[\mathrm{A}\ ^2\Sigma^+\cdots 5s\sigma,5p\sigma,4d\sigma]^1\Sigma(0)$ states ($\Omega=0$ again is indicated by the positive β-parameter) lies in the outer well near 2.2 Å internuclear distance and the nuclear wave functions of these states at the respective energy have a considerable overlap integral with free wave functions starting at the inner wall of the diabatic potential of the V $^1\Sigma^+$ state (see Fig. 4 of Ref. 14).

In contrast with the wealth of processes described above (except one, channels leading to excited chlorine have been neglected here) for REMPI processes via pure Rydberg states in the vicinity of the B $^1\Sigma^+$ state, direct ionization in a REMPI[2+1] process is by far the dominant channel. On the

other hand, recent observations by Kvaran *et al.* in mass resolved REMPI[2+n] (n=1,2) spectra of jet cooled HCl showed a sharp increase in the Cl^+- and H^+-ion signals for single Q-branch lines in the transition bands $F\ ^1\Delta_2 \leftarrow X\ ^1\Sigma^+(1,0)$ [Q(8)] and $f\ ^3\Delta_2 \leftarrow X\ ^1\Sigma^+(0,0)$ [Q(5)]. These were ascribed to near resonance interactions with single rotational levels in the $V\ ^1\Sigma^+$ state, i.e., $v'=14$, $J'=8$,[16] and $v'=8$, $J'=5$,[15] respectively. Indeed, the energy difference between the levels is 17.7 cm^{-1} for the triplet state and 11.3 cm^{-1} for the singlet state. This notion is summarized in Eq. (5).

$$\begin{aligned} &\mathrm{HCl}(\mathrm{B}\ ^1\Sigma^+, v', J') \xrightarrow{h\nu} \mathrm{H}^+, \mathrm{Cl}^+, \mathrm{Cl}^-, \mathrm{HCl}^+(v^+ \leq 12) \\ &\quad \updownarrow \\ &\mathrm{HCl}(\mathrm{f/F}\ ^{3/1}\Delta_2, v', J') \xrightarrow{h\nu} \mathrm{HCl}^+(v^+ < 5). \end{aligned} \tag{5}$$

Here, the upper equation is a shortened version of Eq. (1). In order to shed more light on this matter, we studied the spatial proton velocity distribution of the respective transitions, since the characteristic features for the photodissociation of the $V\ ^1\Sigma^+$ being responsible for the outer well of the $B\ ^1\Sigma^+$ state mentioned above (Eqs. (2)–(4)) should be clearly visible in the product kinetic energy distribution. Furthermore, the proton angular distribution should be describable as the product of a distribution with a negative β-parameter and one with the β-parameter of the subsequent photodissociation, since the alignment of the molecules in the f/F Rydberg states should be according to two subsequent perpendicular ($\Delta\Omega=1$) transitions.[25] For the transition $f\ ^3\Delta_2 \leftarrow X\ ^1\Sigma^+(0,0)$ we find a drastic change in the shape of the speed distribution for the Q(5) line compared to the neighboring transitions. The Q(1–4) and Q(6) lines are characterized by an H^+ speed distribution showing the features of $H(n=2)+Cl(^2P_{3/2})$ production and $HCl^+(5 \leq v^+ \leq 8)$ photodissociation. In contrast, the Q(5) line shows $H(n=2)+Cl(^2P_{1/2})$ and ion-pair production, but the HCl^+ photodissociation channel has not increased in intensity. A closer look at the circumstances will reveal that the fragmentation dynamics of the absorption processes after the two-photon step can be explained by Franck–Condon factors consistent with the nuclear wave function in the B state at the energy of the $f\ ^3\Delta_2$ ($v'=0$) state having only a small fraction in the inner well of the double minimum state. Concerning the transition $F\ ^1\Delta_2 \leftarrow X\ ^1\Sigma^+(1,0)$ we found no H^+ ions for transitions other than the Q(8) line. The speed distribution emerging from this process is the same as the respective Q(8) and Q(7) lines of the transition $V\ ^1\Sigma^+ \leftarrow X\ ^1\Sigma^+(14,0)$.

II. EXPERIMENTAL

The experimental setup has been described in two recent publications.[26,27] Thus, here we will give only a short summary and the facts relevant to the current experiment. A homebuilt TOF spectrometer mounted to a commercial three-dimensional (3D) imaging detector consisting of a two stage micro channel plate and a delay line anode (RoentDek)[28,29] in a stainless steel vacuum vessel is the heart of the 3D velocity mapping apparatus. The TOF spectrometer consists of a pulsed nozzle (General Valve, Series 9 pulsed valve) mounted to a plate, five ring electrodes comprising the acceleration region of approximately 5 cm (depending on the laser path), a tube of 10 cm length serving as a field free drift region and two meshes separating the acceleration from the drift region and the drift region from the detector. The potentials of the Einzel-lens electrode and the acceleration region were supplied by two voltage supplies (Stanford Research System, Model PS350) and measured to five digits precision by a Keithley 2000 voltmeter. The vacuum chamber is pumped by two turbo molecular pumps (Pfeiffer TMU 260 P, 220 l/s) forepumped by a rotary vane pump filled with PFPE oil. Without any gas flow, the background pressure is approximately 10^{-7} mbar. When the nozzle is operating, the integral pressure is of the order of 10^{-5} mbar.

Pure HCl with a stagnation pressure of approximately 400 mbar was expanded through the pulsed nozzle (400 μm orifice) and a dye laser [Nd:YAG (Yttrium Aluminum Garnet) pumped Scanmate 2, Coherent] operating around 487.6 nm or 468.3 nm and frequency doubled by a BBO crystal was focused by an f=0.3 m lens ca. 5 mm downstream of the nozzle orifice. For the measurements reported here, the delay of the nozzle trigger was chosen such that the laser pulse came a few hundred microseconds before the gas pulse, in order to have only gas from the room temperature background making the nozzle a mere gas inlet. Cooling of the gas in a supersonic expansion must be avoided in order to maintain a significant population of HCl in rotational states up to J=8. The repetition rate of the experiment was between 5 and 20 Hz, depending on the ion signal.

The pulses coming from the ends of the DL were differentially amplified (KSU EDL DLA800), recorded by a four channel oscilloscope (Waverunner 6050, Quad 5 Gs/s). The individual pulses were fitted by Gaussians in order to obtain the center of the peaks yielding the times with nearly 100 ps precision. These were used to obtain the time and position of the individual ion impacts from which the velocity vectors were computed using a forward simulation by the program SimIon© based on the dimensions of the spectrometer and the measured voltages.

III. EXPERIMENTAL RESULTS AND DISCUSSION

Figure 1 shows the potential energy curves that are relevant to the following discussion of the experimental data. Also, keep in mind Eqs. (2)–(4) which sum up the mechanisms for the dynamics in the H^+ channel. The two- and three-photon energies for the two processes studied are indicated in Fig. 1 by the hatched areas, the lower energy corresponding to the wavelength for the REMPI process through $f\ ^3\Delta_2 \leftarrow X\ ^1\Sigma^+$. The $B\ ^1\Sigma^+$ potential has been adapted from Ref. 30 and the wave function has been calculated by the Numerov method for the eigenvalue closest to the two-photon energy. Our eigenvalue is 10.332 eV compared to 10.356 eV for the two-photon energy. The fact that the wave function has only six nodes indicates already that the outer well of the potential is not sufficient for spectroscopic purposes. Comparison with the data of Green *et al.* confirms this notion[12] and work is being done to calculate an improved version of this potential.[31] However, it seems to be a good

TABLE I. Constants used in this study.

Property	Value (eV)
Electron affinity Cl[a]	3.613 04
$E(Cl(^2P_{1/2}))$ [b]	0.109 397 6
D(HCl)[c]	4.4321
$D(HCl^+)$ [c]	4.6540
$E(H(n=2))$ [d]	10.199
$\omega_e/\omega_e x_e X\ ^2\Pi(HCl^+)$ [e]	2673.69/52.537 cm^{-1}

[a]Reference 32.
[b]Reference 33.
[c]Reference 34.
[d]Reference 35.
[e]Reference 36.

sketch of the reality that nicely illustrates the probability density for the internuclear distance consistent with our data (*vide infra*) and the rotational constants in Ref. 12 which indicate that the level position with respect to the barrier is more or less correct. This is the only important point here. The rotational constants in Ref. 12 clearly show that v=8 is the last level of the $V\ ^1\Sigma^+ \leftarrow X\ ^1\Sigma^+$ propagation with an almost constant B_v which rises strongly for v=9 and even more for v=10, indicating smaller internuclear distances.

The $F\ ^1\Delta_2$ and $f\ ^3\Delta_2$ (blue) potentials are Morse potentials constructed from the spectroscopic data of Green *et al.*[10–12] The dashed curve in Fig. 1 is the $X\ ^2\Pi$ *ab initio* ground state of HCl^+ calculated by Pradhan *et al.*[5] Furthermore, the dissociative Rydberg states (red curves) are their *ab initio* curves shifted to the respective dissociation energy. The bound Rydberg states with an $A\ ^2\Sigma^+$ ion core have been obtained using the quantum defects of Lefebvre–Brion and Keller and the ionic *ab initio* curve of Pradhan *et al.*[5,7] The values used in these procedures and the calculation of the proton kinetic energies discussed below are listed in Table I.[32–36]

A. Proton formation in the $f\ ^3\Delta_2 \leftarrow X\ ^1\Sigma^+(0,0)$ band system

In Fig. 2 we show a meridian plot[37] of the spatial velocity distribution of H^+ ions emerging from the two-photon absorption $f\ ^3\Delta_2 \leftarrow X\ ^1\Sigma^+(0,0)$ via the Q(2) and Q(5) transitions and subsequent absorption of one or two more photons. For the Q(2) line one can clearly see two processes, the "faster" of which has a large and positive β-parameter. The anisotropy of the slower ions is not discernible in this figure because the points are too dense (see also Table II). In the plot of the Q(5) line the faster ions are absent but instead ions belonging to a third process are visible much closer to the "slow" ions which appear like a corona to these.

Figure 3 shows the H^+ speed distributions for all Q-branch transitions recorded (J=2–6). Phenomenologically, the comparison of the details for each rotational line shows three features.

(i) The "fast" channel peaking at 17 000 m/s corresponds to the photodissociation of HCl^+ in $v^+=5-8$ and decreases strongly in relative intensity for J=5.

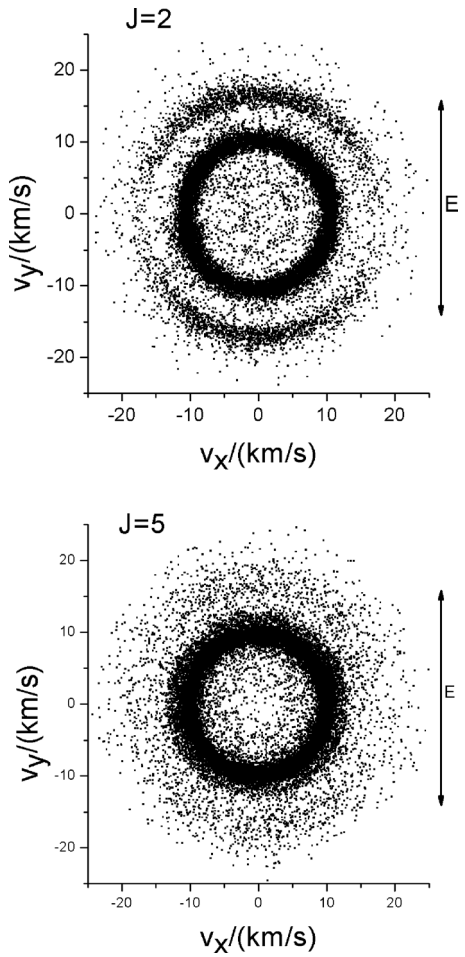

FIG. 2. Meridian plots of the proton velocity distributions for the REMPI process through the Q(2) and Q(5) transitions of the $f\ ^3\Delta_2 \leftarrow X\ ^1\Sigma^+(0,0)$ band.

(ii) The "slow" channel at 10 000 m/s shows a gradual shift to a lower kinetic energy when J=5 is approached, i.e., for J=6 and J=4 the peak positions lie in between the positions for J=2,3 and J=5. The difference in kinetic energy release corresponds to the generation of electronically excited H atoms (H(n=2)) together with ground state ($^2P_{3/2}$) or spin orbit excited ($^2P_{1/2}$) chlorine, respectively.

(iii) The slow peak shows a shoulder for J=5 (the "corona") at ca. 12 000 m/s. Its kinetic energy release corresponds to the ion-pair dissociation.

Generally, the anisotropy of these multiphoton processes can be described by $P(\theta)=1/4\pi(1+\Sigma_j\beta_j P_j(\cos\theta))\cdot\sin\theta$, (j=2,4,⋯2N for N photons). Instead of using this expression directly for the data analysis, we chose to fit the angular distribution $dP(\theta)/d\cos(\theta)$ by a model function that is a product of three independent dipole distributions having individual β_2 parameters.

$$\frac{dP(\theta)}{d\cos(\theta)} = \text{const.} \cdot \prod_{i=1}^{3} (1 + \beta_{2,i} \cdot P_2(\cos(\theta))). \quad (6)$$

Physically, this means that each photon contributes its own β_2-parameter which is of course in general a simplification

TABLE II. Summary of anisotropy parameters for the H^+ distributions for all Q lines of the f $^3\Delta_2 \leftarrow$ X $^1\Sigma^+(0,0)$ REMPI[2+n] process.

f $^3\Delta_2 \leftarrow$ X $^1\Sigma^+(0,0)$		Q(2)	Q(3)	Q(4)	Q(5)	Q(6)
H(n=2)+Cl	$\beta_{2,1}/\beta_{2,2}/\beta_{2,3}$	−0.71/0.84/−0.71	1.21/−0.8/−0.8	−0.4/−0.4/0.72	0.05/0.05/0.05	−0.15/−0.15/−0.2
	$\beta_2/\beta_4/\beta_6$	−0.67/−0.26/0.11	−0.5/−0.58/0.2	−0.15/−0.2/0.03	0.14/0/0	−0.42/0.03/0
H^++Cl^-	$\beta_{2,1}/\beta_{2,2}/\beta_{2,3}$	⋯	⋯	⋯	−0.3/−0.3/0.05	⋯
	$\beta_2/\beta_4/\beta_6$	⋯	⋯	⋯	−0.59/0.04/0	⋯
HCl^+	$\beta_{2,1}/\beta_{2,2}/\beta_{2,3}$	1.28/0.64/−0.35	0.84/0.8/−0.5	1.28/0.3/−0.5	1.29/0.12/−0.3	1.24/−0.14/−0.14
Photolysis	$\beta_2/\beta_4/\beta_6$	1.47/−0.0/−0.07	1/−0.21/−0.09	0.97/−0.3/−0.05	1.02/−0.19/−0	0.94/−0.17/0.01

for the two-photon step, but first, it will help to unravel some of the details of the dynamics and second, in the special case here, this description is justified by the following argument: for a two-photon transition from $\Omega=0$ to $\Omega=2$ or vice versa the only allowed spherical transition tensor components are $T^2_{\pm 2}$. Thus, the alignment of the final state for linearly polarized light is such that, assuming this state would dissociate rapidly, the photofragment distribution anisotropy would be characterized by $\beta_2=-10/7$ and $\beta_4=3/7$,[38] which is equivalent to two individual $\beta_{2,i}=-1$ (i=1,2). This can be verified using Eqs. (7)–(9) setting $\beta_{2,3}=0$. Therefore, assuming that the subsequent photodissociation of the aligned state is independent of the two-photon step, the resulting photofragment angular distribution is a product of the dipole distribution for the one-photon photodissociation characterized by one β_2 and two more dipole distributions characterized by negative β_2 parameters (−1 in the limit of instantaneous dissociation). The reason that we use Eq. (6) for the fit and not the usual representation as a sum of Legendre polynomials and then calculate the individual $\beta_{2,i}$ from this is that in that latter case one has to solve the nonlinear system of equations given by Eqs. (7)–(9) for the $\beta_{2,i}$-parameters. This always yields multiple solutions of which normally all except one are complex or not in the allowed interval $-1 \leq \beta_{2,i} \leq 2$, but in some cases the result is not unique.

$$\beta_2 = 5 \cdot \frac{7 \cdot (\beta_{2,1}+\beta_{2,2}+\beta_{2,3}) + 2 \cdot (\beta_{2,1}\beta_{2,2}+\beta_{2,1}\beta_{2,3}+\beta_{2,2}\beta_{2,3}) + 3 \cdot \beta_{2,1}\beta_{2,2}\beta_{2,3}}{35 + 7 \cdot (\beta_{2,1}\beta_{2,2}+\beta_{2,1}\beta_{2,3}+\beta_{2,2}\beta_{2,3}) + 2 \cdot \beta_{2,1}\beta_{2,2}\beta_{2,3}}, \tag{7}$$

$$\beta_4 = \frac{9}{11} \cdot \frac{22 \cdot (\beta_{2,1}\beta_{2,2}+\beta_{2,1}\beta_{2,3}+\beta_{2,2}\beta_{2,3}) + 12 \cdot \beta_{2,1}\beta_{2,2}\beta_{2,3}}{35 + 7 \cdot (\beta_{2,1}\beta_{2,2}+\beta_{2,1}\beta_{2,3}+\beta_{2,2}\beta_{2,3}) + 2 \cdot \beta_{2,1}\beta_{2,2}\beta_{2,3}}, \tag{8}$$

$$\beta_6 = \frac{90}{11} \cdot \frac{\beta_{2,1}\beta_{2,2}\beta_{2,3}}{35 + 7 \cdot \beta_{2,1}\beta_{2,2} + 7 \cdot \beta_{2,1}\beta_{2,3} + 7 \cdot \beta_{2,2}\beta_{2,3} + 2 \cdot \beta_{2,1}\beta_{2,2}\beta_{2,3}}. \tag{9}$$

Figure 4 shows the angular anisotropy of the protons emerging from the excited H atom [case ii and the HCl^+ photolysis channel (case i)] for the Q(3) line. A summary of the anisotropy parameters for both representations is given in Table II. From this one can learn that for the unperturbed transitions Q(2) and Q(3) there is always a perpendicular contribution ($\beta<0$) to the H(n=2) channel that results from the alignment of the intermediate state, since, as explained above, the two-photon transition from an $\Omega''=0$ to an $\Omega'=2$ state can be regarded as two subsequent perpendicular transitions for which $\Delta\Omega=1$.[38]

This effect decreases when J=5 is approached and for J=5 itself the angular distribution becomes isotropic. Concerning the peak for the HCl^+ photolysis (case i) which is very small (<5%) for the Q(5) line, the anisotropy is not altered at all for any of the rotational lines. This, together with the fact that it does not increase in intensity, means that this process is solely characteristic for the pure Rydberg state at this energy. Here, the perpendicular contribution is much smaller than for the H(n=2) channel (case ii) which suggests that the autoionization process as well as the HCl^+ photodissociation are dominated by parallel transitions. The fact that the density at the poles is not very much smaller than would be expected for a process with only positive β-parameters (see Fig. 4, lower panel) indicates that the duration of the process after the formation of the molecular ion is on the order of the rotational period. The H(n=2) peak is a sum of equal contributions of $Cl(^2P_{1/2})$ and $Cl(^2P_{3/2})$ for the Q(4,6) lines, while only $Cl(^2P_{1/2})$ contributes (within the given resolution) to the Q(5) line. The relative integral for the HCl^+ photolysis peak is lower for Q(4,6) than for Q(2,3) and reduces to approximately 1/5 for the Q(5) line (see Fig. 3), and the ratio of Cl^+ to HCl^+ ions gradually increases when the Q(5) line is approached as reported in Ref. 16. The fact that the angular distribution for the H(n=2) channel does not show the mark of the initial double perpendicular two-photon transition we think is due to interchange of angular momentum between electrons and nuclei by going from

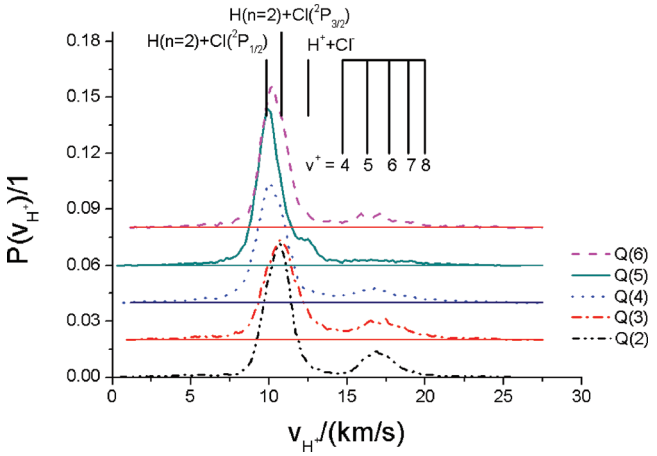

FIG. 3. Speed distributions for the protons generated in the REMPI process through the Q(2–6) transitions of $f\ ^3\Delta_2 \leftarrow X\ ^1\Sigma^+(0,0)$ band.

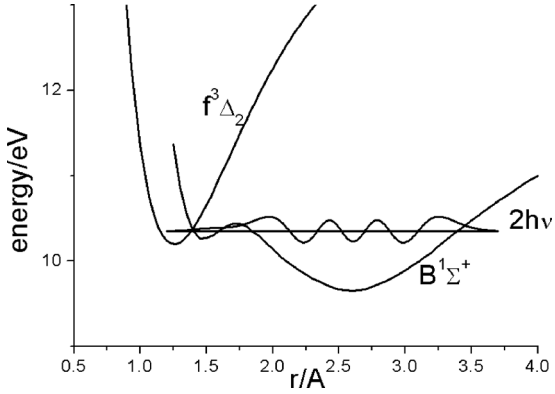

FIG. 5. Potential energy curves for the $f\ ^3\Delta_2$ and $B\ ^1\Sigma^+$ states derived from spectroscopic data in Refs. 10–12 and reproduced from Bruna *et al.* (Ref. 30), respectively. The Numerov wave function is shown for the eigenvalue closest to the two-photon energy.

$\Omega=2$, N=6 to $\Omega=0$, N=J=8 in the nonadiabatic transition (at least two negative β-parameters should remain like for the other rotational lines as explained above). Similar effects have been described by Kable *et al.* for HCO when the combination of angular momenta is changed in a nonadiabatic transition prior to dissociation.[39] Moreover, the H(n=2) distribution becomes completely isotropic and the anisotropy for the ion-pair peak can be described by a single negative β_2-parameter. We see the same effect for the H(n=2) channel in the singlet transition $F\ ^1\Delta_2(v'=1,\ J'=8) \leftarrow X\ ^1\Sigma^+(v'=0,\ J'=8)$, but not for the HCl^+ photodissociation which we interpret in terms of the time the nuclei have to react to the changing of the electronic configuration (*vide infra*).

Kvaran *et al.* observed no spectral shifts of peak positions that could be a consequence of near resonance interactions between the $f\ ^3\Delta_2$ and the $V\ ^1\Sigma^+(v'=8)$ levels and they estimated the fraction $|c|^2$ of the Rydberg part of the wave function to be 0.987 for $J'=5$ from their ion intensity data.

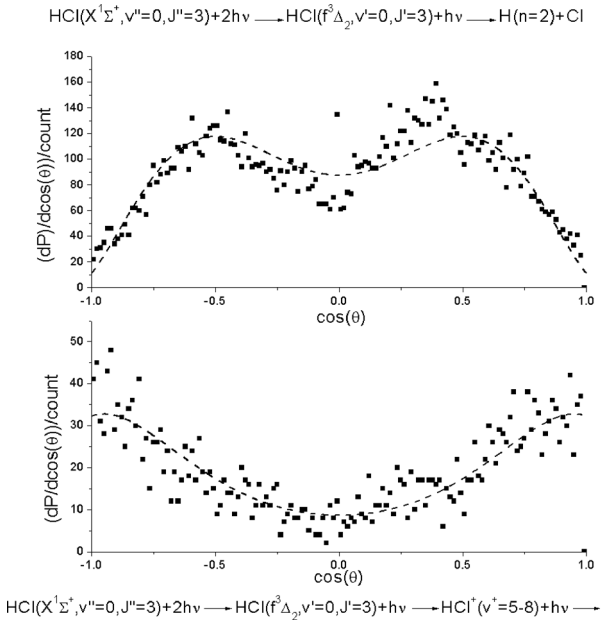

FIG. 4. Angular distributions for the slow and fast channel of the Q(3) line (squares). The least-squares fit is shown as a dashed line.

This shows the weakness of the interaction ($\Delta E_{f\text{-}V}=-57.5$, 17.7 and 105.4 cm^{-1} for $J'=4$, 5, and 6).[16] However, the strong increase in the H^+ ion signal relative to the HCl^+ signal is due to the much higher dissociation probability of the V state and not to a strong coupling of the two states. This means that the HCl^+ photodissociation via the Rydberg state remains more or less unaltered for J=5 and is only seemingly diminished in Fig. 3. Also, the near resonance does not show an imprint on the Q(5) line of the $V\ ^1\Sigma^+ \leftarrow X\ ^1\Sigma^+(8,0)$ band in the form of an enhancement of the HCl^+ ion signal, the main channel for all pure Rydberg states.[16]

It is worthwhile to stress that while no effect is noticeable in the peak intensities of the $V\ ^1\Sigma^+(v'=8) \leftarrow X\ ^1\Sigma^+(v''=0)$ absorption spectrum, the dynamical picture is completely altered for the photorupture. Here, the small near resonance interaction has the drastic effect described above. This shows what sensitive tool dynamical studies are to study such small near resonance effects.

The wave function shown in Figs. 1 and 5 for the eigenvalue closest to the two-photon energy on the *ab initio* potential of Bruna *et al.*[30] explains the phenomena described above very well, since a small fraction of the nuclear wave function in the inner well of the $B\ ^1\Sigma^+$ state will suppress further photon absorption from this region. Consequently, subsequent photon absorption must essentially occur from large internuclear distances on the right hand side of the barrier. However, the Franck–Condon factor for the transition from the right hand side of the barrier to the $[^4\Pi\cdots 4s]^3\Pi_0$ state which has been identified[13,14] previously as the state that autoionizes to the higher vibrational states of HCl^+ is very low or vanishes completely. This explains why no extra HCl^+ photodissociation occurs due to the near resonance. As this $^3\Pi_0$ state is also believed to produce H(n=2) with $Cl(^2P_{3/2})$ as the partner fragment via a nonadiabatic transition to one of the bound $[A\ ^2\Sigma^+\cdots 4s]\Sigma$ states, this explains also why no extra H(n=2) are generated together with ground state chlorine. In contrast, excitation of a repulsive Rydberg state having a $(2)^2\Pi$ ion core and a 4s Rydberg electron is possible Franck–Condon-wise and explains why only $Cl(^2P_{1/2})$ is formed as the hydrogen's partner

fragment.[14,19] The formation of the ion-pair has been explained by Romanescu *et al.* by excitation to a bound $^1\Sigma^+(0^+)$ Rydberg state having an A $^2\Sigma^+$ ion core and a 5sσ, 5pσ, or 4dσ Rydberg electron and subsequent predissociation to the diabatic curve of the V $^1\Sigma^+$ state at small internuclear distances (see Fig. 4 in Ref. 14). They verified this by calculating the overlap integrals using Numerov integration of the Schrödinger equation over the same *ab initio* B $^1\Sigma^+$ potential of Bruna *et al.* shown in Figs. 1 and 5. Since this feature can be seen for all vibrational states, we believe that the outer well being not deep enough resulting in two vibrational quanta missing has no significant effect on this result. Here, $\Delta\Omega=0$ followed from the observation that for the V $^1\Sigma^+\leftarrow$X $^1\Sigma^+(v'\geq 11,0)$ Q(0) lines the β-parameter is 2, since in this case no alignment can occur.[14,19] Since we see the dynamics connected with the outer well exclusively at the energy for the transition to the f $^3\Delta_2$ state, the ion-pair channel can indeed be only accessed from large internuclear distances. We think that the observed anisotropy, which is different from that observed for higher vibrational states by Romanescu *et al.* and in our laboratory, is due to a perpendicular transition from the V $^1\Sigma^+$ to an $\Omega=1$ state, because (i) there is no positive β component and (ii) it is likely that the alignment of the double perpendicular two-photon transition is lost in the nonadiabatic transition from the f $^3\Delta_2$ to the V $^1\Sigma^+$ state. For the latter point see the discussion for the F $^1\Delta_2$ band system below (III B). The fact that we found H^+/Cl^+ production for the adjacent "off-resonance" Q-lines at all needs further clarification as well. Kvaran *et al.* also found H^+ and Cl^+ and attributed this to predissociation of the triplet Rydberg states to ground state atoms, to dissociation of a superexcited bound state yielding excited chlorine and to photodissociation of HCl^+ yielding H^+ (see Fig. 1 in Ref. 16). For the first mechanism [(viii) in Ref. 16] we found no evidence (the laser power of ca. 10 μJ/pulse is too low for ionizing H atoms nonresonantly) but we cannot rule it out either. Additionally, it may still contribute to the Cl^+ signal which we cannot study here due to interference from the huge HCl^+ signal. The Cl^+ from the second of these dissociation mechanisms [(ix) in Ref. 16] is not detected by us, but we believe that it is at least partly Cl(4s) emerging from excitation of the gateway state $[^4\Pi\cdots 4s]$ to autoionization $^3\Pi_\Omega$ [process (i) in Ref. 16, *vide infra*]. The parameter γ in that study denoting the ratio of Cl^+ produced from photodissociation of the Rydberg state to the Cl^+ produced from photodissociation of the V state is equal to zero (or at least negligible) for $J'=5$. This is what we also see for the H^+ channel, since the spatial distributions are completely different for the off-resonant rotational lines.

However, as the F $^1\Delta_2$ state only shows significant fragmentation for the near-resonant Q(8) line (*vide infra*) and Kvaran *et al.* found small but significant photolysis for other triplet states as well, there could be some triplet state opening the dissociation and autoionization channel. We believe this to be due to the fact that the transition is spin allowed, since the gateway state to autoionization is supposed to be a $^3\Pi_0$ state. However, in our case, it must be the $^3\Pi_2$ state of the $^4\Pi$ ion core group, since the observed β-parameter for the process is large and positive. This explains the formation of H(n=2) together with $Cl(^2P_{3/2})$, since the $^3\Pi_\Omega$ state crosses the potential curves of the bound $[A\ ^2\Sigma^+\cdots 4s]$ state, and the formation of Cl(4s) atoms since it asymptotically correlates with H+Cl(4s). These Cl(4s) have probably been detected by Kvaran *et al.* as Cl^+ ions for the triplet states not near any resonance with the V $^1\Sigma^+$ state. Since the Franck–Condon factors should be as small as for the singlet states, the direct ionization is still by far the dominating process.

The fragmentation dynamics presented in this section are summarized in Eq. (10). Note that the upper part of Eq. (10b) can be regarded as more or less unaltered by the small interaction although it looks strongly diminished in Fig. 3. This is because the small fraction transferred to the V-state is so effectively dissociated.

$$\mathrm{HCl}\xrightarrow{2h\nu}\mathrm{HCl}(f\ ^3\Delta_2, J'\neq 5)\xrightarrow{h\nu}\mathrm{HCl}([^4\Pi\cdots 4s]^3\Pi)\rightarrow\begin{cases}\mathrm{HCl}^+(v^+\geq 5)\\ \mathrm{H(n=2)+Cl}\ (^2P_{3/2})\\ \mathrm{H+Cl(4s)}\end{cases}, \tag{10a}$$

$$\mathrm{HCl}\xrightarrow{2h\nu}\mathrm{HCl}(f\ ^3\Delta_2, J'=5)\xrightarrow{h\nu}\mathrm{HCl}([^4\Pi\cdots 4s]^3\Pi)\rightarrow\begin{cases}\mathrm{HCl}^+(v^+\geq 5)\\ \mathrm{H(n=2)+Cl}\ (^2P_{3/2})\\ \mathrm{H+Cl(4s)}\end{cases} \tag{10b}$$

$$\updownarrow$$

$$\mathrm{HCl}(V\ ^1\Sigma^+, v'=8, J'=5)\xrightarrow{h\nu}\mathrm{HCl}([A\ ^2\Sigma^+\cdots nl\sigma])\rightarrow\mathrm{HCl}(V\ ^1\Sigma^+)\rightarrow\mathrm{H}^+ + \mathrm{Cl}^-$$

$$\xrightarrow{h\nu}\mathrm{HCl}([(2)^2\Pi\ldots .4s])\rightarrow\mathrm{H(n=2)+Cl}(^2P_{1/2}).$$

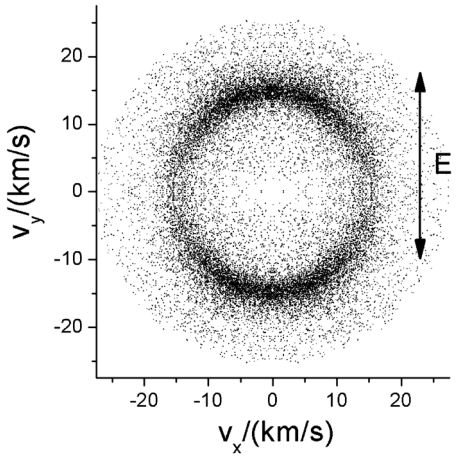

FIG. 6. Symmetrized meridian projection (for details see Ref. 37) of the 3D velocity distribution of H^+ ions resulting from the 2+1 REMPI process through the F $^1\Delta_2 \leftarrow$ X $^1\Sigma^+(1,0)$ Q(8) transition.

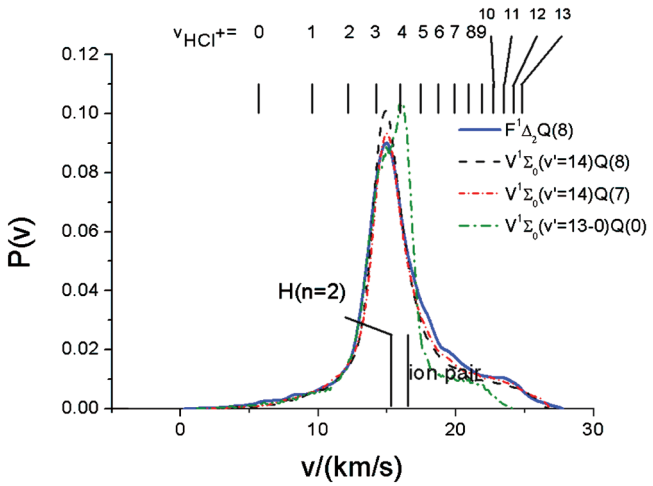

FIG. 7. Comparison of the H^+ speed distributions for the transitions F $^1\Delta_2 \leftarrow$X $^1\Sigma^+(1,0)$ Q(8), V $^1\Sigma^+ \leftarrow$X $^1\Sigma^+(14,0)$ Q(8,7), and V $^1\Sigma^+ \leftarrow$X $^1\Sigma^+(13,0)$ Q(0).

B. Proton formation in the F $^1\Delta_2 \leftarrow$X $^1\Sigma^+(1,0)$ band system

Figure 6 shows a symmetrized meridian projection[37] of the 3D point cloud of H^+ ions in velocity space as measured for the REMPI process via the F $^1\Delta_2 \leftarrow$X $^1\Sigma^+(1,0)$ Q(8) two-photon transition.

The overall positive β-parameter is clearly observable. Due to the higher photon energy as in Sec. III A, the fast ions belonging to the HCl^+ photolysis almost merge with the slower ions composed of the dissociation into the ion-pair and in H(n=2)+Cl $^2P_{1/2/(3/2)}$ [for a summary of the H^+ producing mechanism see Eqs. (2)–(4) in the Introduction]. This is because the latter result from a three-photon dissociation of the neutral molecule whereas the first emerge from a one-photon dissociation of the molecular ion and therefore the available energy of the latter decreases relative to the first as the photon energy increases. It should be noted that the Q(8) transition to the F $^1\Delta_2$(v′=1) state was the only one out of the Q-branch transitions for that we found an H^+ signal considerably above the background level.

Figure 7 shows that the kinetic energy profile for the H^+ ions emerging from the transition to the F state (v′=1, J′=8) being in near resonance ($\Delta E = 11.3\ cm^{-1}$) (Ref. 15) with the respective rotational level in the V state (v′=14, J′=8) is the same as the one resulting from the REMPI process via the V state. Given that these fragmentation dynamics are a fingerprint for the outer well of the B $^1\Sigma^+$ state, this constitutes a direct observation for the resonance mediated mechanism proposed by Kvaran and co-workers who measured the relative ion intensities using mass resolved REMPI-TOF (time of flight). We do not show the H^+ distribution for the Q(0) transition of the V $^1\Sigma^+ \leftarrow$X $^1\Sigma^+(14,0)$ vibrational band, because the signal was not discernible against the background. This reflects the observation already mentioned by Green *et al.* that the v′=14 rotational progression shows unnaturally small relative line intensities not explainable by Frank–Condon factors in addition to abnormal rotational energy shifts. This is attributed to strong Rydberg-valence interactions with the nearby E $^1\Sigma^+$ and g $^3\Sigma^-$ states.[12] Presumably, this is also why Loock *et al.* left out the v′=14 state in their study. However, to the best of our knowledge, this is the first time the H^+ speed distribution for the REMPI process via this vibrational state of the V $^1\Sigma^+$ progression has been measured. Comparison with the also shown distribution resulting from the REMPI process via the Q(0) transition of the V $^1\Sigma^+ \leftarrow$X $^1\Sigma^+(13,0)$ vibrational band shows that the v′=14 distributions exhibits a markedly diminished ion-pair peak. This is in accord with the trend observed by Loock *et al.* that the ion-pair peak diminishes strongly by going from the v′=13 to the v′=15 vibrational state of the V state.

Figure 8 depicts the angular distributions for the H(n=2) channel and the HCl^+ photodissociation channel for the REMPI transition F $^1\Delta_2 \leftarrow$X $^1\Sigma^+(0,1)$Q(8). Table III summarizes the anisotropy parameters for the relevant transi-

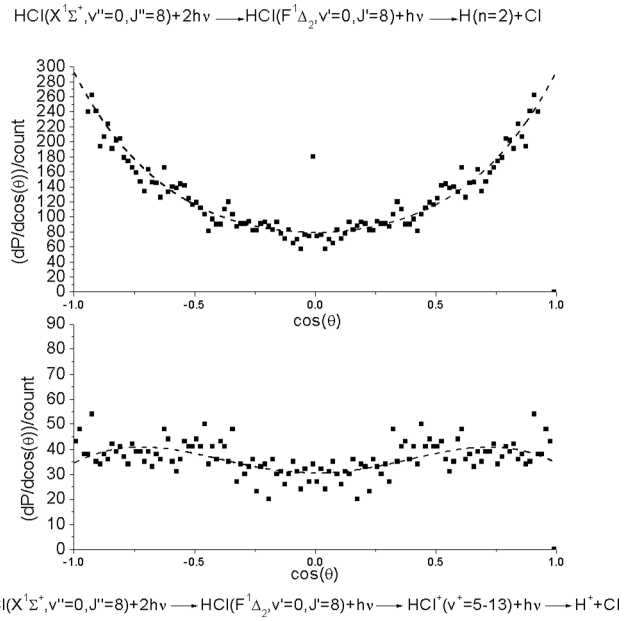

FIG. 8. Angular distributions for the H(n=2) and HCl^+ photodissociation channel for the transition F $^1\Delta_2 \leftarrow$X $^1\Sigma^+(0,1)$Q(8).

TABLE III. Summary of anisotropy parameters for the H^+ distributions for the REMPI[2+n] processes shown in Fig. 7.

		Transition		
		F $^1\Delta_2 \leftarrow$ X $^1\Sigma^+(1,0)$Q(8)	V $^1\Sigma^+ \leftarrow$ X $^1\Sigma^+(14,0)$Q(8)	V $^1\Sigma^+ \leftarrow$ X $^1\Sigma^+(14,0)$Q(7)
H(n=2)+Cl	$\beta_{2,1}/\beta_{2,2}/\beta_{2,3}$	0.85/0.07/0.07	0.91/−0.5/−0.5	0.77/−0.16/−0.16
	$\beta_2/\beta_4/\beta_6$	1.0/0.06/0.0	−0.21/−0.31/0.1	0.42/−0.11/0.0
HCl^+	$\beta_{2,1}/\beta_{2,2}/\beta_{2,3}$	0.79/−0.4/−0.4	0.7/−0.64/−0.64	1.13/−0.65/−0.65
Photolysis	$\beta_2/\beta_4/\beta_6$	−0.05/−0.22/−0.03	−0.64/−0.2/0.07	−0.33/−0.49/0.14

tions. It is noteworthy that the anisotropy for the HCl^+ photolysis remains unaltered for all three transitions, whereas the H(n=2) channel seems to lose the information about the twofold perpendicular two-photon transition completely, i.e., the negative β-parameter that should arise due to the expected alignment is absent. Above we observed the same effect for the triplet transitions in Sec. III A. We believe that the reason for this is the exchange of angular momentum of the electrons and nuclei in the nonadiabatic transition to the dissociating state from the final state of the absorption. Kable *et al.*[39] experimentally and theoretically described such effects for the HCO photodissociation where opposite or unexpected photodissociation anisotropies with respect to those expected by the knowledge of the electronic transition occur. Therefore, we think that the observed effect can be interpreted in the following way: the alignment of the molecular axis due the two-photon transition is destroyed in the nonadiabatic transition from the $\Omega=2$ ($F\ ^1\Delta_2$, $f\ ^3\Delta_2$) states to the $\Omega=0$ ($V\ ^1\Sigma^+$) states. Regarding the observations, this means that the transition to the autoionizing $[^4\Pi\cdots 4s]^3\Pi$ state producing vibrationally excited HCl^+ is not so much affected by this as are the channels producing H(n=2) and the ion pair, since it still bears the mark of the initial alignment of the two-photon excitation. We believe that the reason for this is that the ion-pair channel [not resolved for the $^1\Delta_2, v'=1$ and $^1\Sigma^+, v'=14$ transitions (Fig. 7)] and the H(n=2) channel start from larger interatomic distances with the pure ion-pair character of the $V\ ^1\Sigma^+$ state (see Fig. 1). Here, the information about the initial alignment is lost when the combination of N=6 and $\Omega=2$ is switched to N=J=8 and $\Omega=0$. The fact that the distributions of the H^+ emerging from the HCl^+ photolysis, both for the $F\ ^1\Delta_2$ and the $f\ ^3\Delta_2$ transitions, still show the fingerprint of the alignment due to the two-photon transition can be interpreted such that this process is fast compared to the reaction of the nuclei to the switching of the electronic configuration. This seems reasonable, since the Franck–Condon region for the transition to the $[^4\Pi\cdots 4s]^3\Pi$ state is close to the crossing of the potential curves of the F/f states with the B state.

IV. CONCLUSION

In extension of previous work, in this article we investigated the quantum state specific fragmentation behavior of REMPI processes in HCl through the Rydberg states $F\ ^1\Delta_2$ and $f\ ^3\Delta_2$. This has been achieved by measuring the spatial velocity distribution of the H^+ ions emerging from these transitions by means of the 3D velocity map imaging technique. H^+ resulting from the processes (1) $HCl+3h\nu \rightarrow H(n=2)+Cl(^2P_J)$, (2) $HCl+3h\nu \rightarrow H^+ + Cl^-$, and (3) $HCl+3h\nu \rightarrow HCl^+; HCl^+ + h\nu \rightarrow H^+ + Cl$ were monitored.

Basically, the near resonance rotational states in the $f\ ^3\Delta_2$ and $F\ ^1\Delta_2$ states behave identically to the $B\ ^1\Sigma^+$ states in that way that single rotational lines of the REMPI[2+n] (n=1,2) band systems $F\ ^1\Delta_2 \leftarrow X\ ^1\Sigma^+(1,0)$ and $f\ ^3\Delta_2 \leftarrow X\ ^1\Sigma^+(0,0)$ [i.e., Q(8) and Q(5), respectively] show the characteristic fragmentation dynamics of the $V\ ^1\Sigma^+ \leftarrow X\ ^1\Sigma^+$ band system. This proved the suggested mechanism by Kvaran *et al.* that the vicinity in energy of the respective rotational energy levels to those in the $V\ ^1\Sigma^+$ ion-pair state leads to the enhanced fragmentation of the f/F-Rydberg states that they observed by mass resolved REMPI-TOF. Additionally, a series of subtle details concerning the fragmentation dynamics in the investigated states were observed.

Concerning the $f\ ^3\Delta_2 \leftarrow X\ ^1\Sigma^+(0,0)$ band our results show that the additional H^+ for the Q(5) line is generated exclusively via the outer well of the $B\ ^1\Sigma^+$ state belonging to the $V\ ^1\Sigma^+$ part of this adiabatic potential. These consist of H(n=2) atoms with Cl ($^2P_{1/2}$) as cofragment and H^+ of the ion pair $H^+ + Cl^-$. Other Q-branch transitions to rotational states not in resonance with the respective rotational states in the $V\ ^1\Sigma^+$ also undergo fragmentation, but the H(n=2) atoms are produced in coincidence with Cl in the spin orbit ground state.

The $F\ ^1\Delta_2 \leftarrow X\ ^1\Sigma^+(1,0)$ band shows fragmentation exclusively for J=8 as the final state and the kinetic energy distribution has been shown to be the same as for the respective $V\ ^1\Sigma^+ \leftarrow X\ ^1\Sigma^+(14,0)$ transition. The anisotropy observed indicates that the HCl^+ autoionization occurs from a more Rydberg-like electronic configuration as the ion-pair channel and the major part of the H(n=2) channel.

Some details manifesting themselves in spatial fragment anisotropies could not yet fully be assessed. For example the autoionizing state excited from the $f\ ^3\Delta_2$ state cannot be the $^3\Pi_0$ state previously reported as the gateway state for the $^1\Sigma^+$ state fragmentation. Instead, the positive β-parameter indicates that it is the respective $^3\Pi_2$ state. Moreover, the gateway state to the ion-pair dissociation at this energy has to be an $\Omega=1$ state out of the Rydberg series having an $A\ ^2\Sigma^+$ ion core.

In summary, the results obtained in this work confirmed and extended the previously obtained global understanding of the HCl fragmentation process in the $(\Lambda=\Sigma=0)\ ^1\Sigma^+$ manifold to Rydberg states with $\Lambda>0$ and $\Omega>0$.

ACKNOWLEDGMENTS

Financial support by the Deutsche Forschungsgemeinschaft and the Alexander von Humboldt foundation (Grant

No. GE-496/14-2) is gratefully acknowledged. We also thank Constantin Romanescu and Hans-Peter Loock for the informative correspondence.

[1] P. Natalis, P. Pennetreau, L. Longton, and J. E. Collin, Chem. Phys. **73**, 191 (1982).
[2] H. Frohlich, P. M. Guyon, and M. Glass-Maujean, Phys. Rev. A **44**, 1791 (1991).
[3] Q. J. Hu, T. C. Melville, and J. W. Hepburn, J. Chem. Phys. **119**, 8938 (2003).
[4] P. Natalis, P. Pennetreau, L. Longton, and J. E. Collin, J. Electron Spectrosc. Relat. Phenom. **27**, 267 (1982).
[5] A. D. Pradhan, K. P. Kirby, and A. Dalgarno, J. Chem. Phys. **95**, 9009 (1991).
[6] Y.-F. Zhu, E. R. Grant, K. Wang, V. McKay, and H. Lefebvre-Brion, J. Chem. Phys. **100**, 8633 (1994).
[7] H. Lefebvre-Brion and F. Keller, J. Chem. Phys. **90**, 7176 (1989).
[8] M. Bettendorff, S. D. Peyerimhoff, and R. J. Buenker, Chem. Phys. **66**, 261 (1982).
[9] D. S. Ginter and M. L. Ginter, J. Mol. Spectrosc. **90**, 177 (1981).
[10] D. S. Green, G. A. Bickel, and S. C. Wallace, J. Mol. Spectrosc. **150**, 354 (1991).
[11] D. S. Green, G. A. Bickel, and S. C. Wallace, J. Mol. Spectrosc. **150**, 303 (1991).
[12] D. S. Green, G. A. Bickel, and S. C. Wallace, J. Mol. Spectrosc. **150**, 388 (1991).
[13] C. Romanescu, S. Manzhos, D. Boldovsky, J. Clarke, and H.-P. Loock, J. Chem. Phys. **120**, 767 (2004).
[14] C. Romanescu and H.-P. Loock, J. Chem. Phys. **127**, 124304 (2007).
[15] A. Kvaran, H. Wang, K. Matthiasson, A. Bodi, and E. Jónsson, J. Chem. Phys. **129**, 164313 (2008).
[16] A. Kvaran, K. Matthíasson, and H. Wang, J. Chem. Phys. **131**, 044324 (2009).
[17] A. Kvaran, A. Logadóttir, and H. Wang, J. Chem. Phys. **109**, 5856 (1998).
[18] K. Matthíasson, H. Wang, and A. Kvaran, J. Mol. Spectrosc. **255**, 1 (2009).
[19] A. I. Chichinin, C. Maul, and K.-H. Gericke, J. Chem. Phys. **124**, 224324 (2006).
[20] A. I. Chichinin, P. S. Shternin, N. Gödecke, S. Kauczok, C. Maul, O. S. Vasyutinskii, and K.-H. Gericke, J. Chem. Phys. **125**, 034310 (2006).
[21] E. F. van Dishoeck, M. C. van Hemert, and A. Dalgarno, J. Chem. Phys. **77**, 3693 (1982).
[22] K. P. Lawley and R. J. Donovan, J. Chem. Soc., Faraday Trans. **89**, 1885 (1993).
[23] A. J. Yencha, D. Kaur, R. J. Donovan, A. Kvaran, A. Hopkirk, H. Lefebre-Brion, and F. Keller, J. Chem. Phys. **99**, 4986 (1993).
[24] A. G. Suits and J. W. Hepburn, Annu. Rev. Phys. Chem. **57**, 431 (2006).
[25] S. Manzhos, C. Romanescu, H.-P. Loock, and J. G. Underwood, J. Chem. Phys. **121**, 11802 (2004).
[26] S. Kauczok, N. Gödecke, A. I. Chichinin, M. Veckenstedt, C. Maul, and K.-H. Gericke, Rev. Sci. Instrum. **80**, 083301 (2009).
[27] A. I. Chichinin, S. Kauczok, K.-H. Gericke, and C. Maul, Int. Rev. Phys. Chem. **28**, 607 (2009).
[28] O. Jagutzki, V. Mergel, K. Ullmann-Pfleger, L. Spielberger, U. Spillmann, R. Dorner, and H. Schmidt-Bocking, Nucl. Instrum. Methods Phys. Res. A **477**, 244 (2002).
[29] I. Ali, R. Dörner, O. Jagutzki, S. Nüttgens, V. Mergel, L. Spielberger, K. Khayyat, T. Vogt, and H. Bräuning, Nucl. Instrum. Methods Phys. Res. B **149**, 490 (1999).
[30] P. J. Bruna and S. D. Peyerimhoff, in *Ab Initio Methods in Quantum Chemistry*, edited by K. P. Lawley (Wiley, New York, 1987).
[31] H. Lefebvre-Brion (private communication).
[32] V. R. Trainham, G. D. Fletcher, and D. J. Larson, J. Phys. B **20**, L777 (1987).
[33] Yu. Ralchenko, A. E. Kramida, J. Reader, and the NIST ASD Team, NIST Atomic Spectra Database, version 3.1.5, National Institute of Standards and Technology, Gaithersburg, MD, 2008 http://physics.nist.gov/asd3 6 November 2009.
[34] M. Michel, M. V. Korolkov, and K.-M. Weitzel, Phys. Chem. Chem. Phys. **4**, 4083 (2002).
[35] A. A. Radzig and B. M. Smirnoff, *Reference Data on Atoms, Molecules and Ions*, Chemical Physics Vol. 31 (Springer, New York, 1985).
[36] K. P. Huber and G. Herzberg, *Constants of Diatomic Molecules* (Van Nostrand, Reinhold, 1979).
[37] A. I. Chichinin, T. Einfeld, C. Maul, and K.-H. Gericke, Rev. Sci. Instrum. **73**, 1856 (2002).
[38] R. N. Dixon, J. Chem. Phys. **122**, 194302 (2005).
[39] S. H. Kable, J.-C. Loison, D. W. Neyer, P. L. Houston, I. Burak, and R. N. Dixon, J. Phys. Chem. **95**, 8013 (1991).